

Focally Elevated Creatine Detected in Amyloid Precursor Protein (APP) Transgenic Mice and Alzheimer Disease Brain Tissue*

Received for publication, June 9, 2005, and in revised form, October 13, 2005
Published, JBC Papers in Press, November 2, 2005, DOI 10.1074/jbc.C500244200

Meghan Gallant^{†1,2}, Margaret Rak^{†1,3}, Adriana Szeghalmi[†],
Marc R. Del Bigio^{§4}, David Westaway^{||}, Jin Yang[†], Robert Julian^{**},
and Kathleen M. Gough^{†5}

From the [†]Department of Chemistry, University of Manitoba, Winnipeg, Manitoba R3T 2N2, the [§]Department of Pathology, University of Manitoba, Winnipeg, Manitoba R3E 0W3, the ^{||}Centre for Research in Neurodegenerative Diseases, University of Toronto, Toronto, Ontario M5S 3H2, the ^{||}Department of Laboratory Medicine and Pathobiology, University of Toronto, Toronto, Ontario M5G 1L5, and the ^{**}Synchrotron Radiation Center, University of Wisconsin at Madison, Stoughton, Wisconsin 53589

The creatine/phosphocreatine system, regulated by creatine kinase, plays an important role in maintaining energy balance in the brain. Energy metabolism and the function of creatine kinase are known to be affected in Alzheimer diseased brain and in cells exposed to the β -amyloid peptide. We used infrared microspectroscopy to examine hippocampal, cortical, and caudal tissue from 21–89-week-old transgenic mice expressing doubly mutant (K670N/M671L and V717F) amyloid precursor protein and displaying robust pathology from an early age. Microcrystalline deposits of creatine, suggestive of perturbed energetic status, were detected by infrared microspectroscopy in all animals with advanced plaque pathology. Relatively large creatine deposits were also found in hippocampal sections from post-mortem Alzheimer diseased human brain, compared with hippocampus from non-demented brain. We therefore speculate that this molecule is a marker of the disease process.

Alzheimer disease (AD)⁶ is a progressive neurodegenerative disorder characterized by memory loss and dementia. The pathological hallmarks of AD include extracellular deposits of β -amyloid ($A\beta$) peptides derived from the amyloid precursor protein (APP695) and neurofibrillary tangles (NFTs) composed of intracellular bundles of hyperphosphorylated tau protein bound into paired helical filaments (1). Reduced or altered brain metabolism, together with oxidative stress and elevated levels of $A\beta$, are believed to play a crucial role in AD pathology; however, their respective roles in the disease process are still not clear (2–6).

We are using Fourier transform infrared (FTIR) microspectroscopy to examine the brains of TgCRND8 and littermate control (non-Tg) mice (7). FTIR microspectroscopy combines spatial resolution at the IR diffraction limit

with molecular fingerprint information, providing a unique tool for the study of plaques and associated changes *in situ*. The TgCRND8 mouse (8) expresses a double mutant form of human APP695 (with two familial AD mutations, K670N/M671L and V717F) and has both diffuse and congophilic dense-cored plaques, with the cortex and hippocampus affected earliest. Dense-cored plaques are associated with dystrophic neurites and an inflammatory response accompanied by microglial activation. We report here the novel and unexpected discovery of large creatine (Cr) deposits in the hippocampi and cortex of transgenic AD mice and in post-mortem sections of human AD hippocampus.

The creatine-phosphocreatine system plays a key role in energy metabolism in tissues such as neurons with high energy demand (9). Phosphocreatine (PCr), synthesized from Cr and ATP in the mitochondria (site of ATP synthesis), is used to regenerate ATP in the cytosol (site of ATP use) by the mitochondrial and cytosolic isozymes of creatine kinase (CK), respectively, thus helping to maintain ATP homeostasis: $\text{Cr} + \text{ATP} \leftrightarrow \text{PCr} + \text{ADP} + \text{H}^+$.

CK is very sensitive to oxidative stress and appears to be one of the specific targets of post-translational oxidative modification in AD brain tissue (10). CK activity is reduced in excised samples of human AD brain relative to age-matched controls (11, 12). Cultured neurons exposed to $A\beta$ exhibit oxidative stress, including increase in protein carbonyl formation and a decline in CK activity (13). Glucose transport is impaired, and ATP levels are reduced (14); mitochondrial function is disturbed (15).

Following our initial identification of Cr deposits in small IR maps of brain tissue from the four 47-week-old and one 21-week-old TgCRND8, we mapped the complete hippocampus in sections from sixteen animals (Tg and non-Tg littermates from two different mouse lines expressing the same double mutant form of APP695) and discovered extensive Cr load in all Tg mice. Large deposits of Cr were also identified in hippocampal sections from post-mortem AD human brain. These deposits are absent or significantly lower in age-matched control mice and in non-demented post-mortem human hippocampus; thus we speculate that their presence is an important and hitherto unsuspected marker of the disease process.

MATERIALS AND METHODS

Transgenic Mice—In the first study, Tg(K670N/M671L+V717F)8 (C3H/C57) mice and non-transgenic littermates were sacrificed at 21 weeks (three TgCRND8 and five non-Tg) and at 47 weeks (four TgCRND8 and four non-Tg). Following the detection of Cr in the transgenics, an additional 16 mice, aged 34–89 weeks, were examined. This set included six pairs of TgCRND8 and non-Tg littermates, as well as two pairs of Tg(K670N/M671L+V717F)19959 and their non-Tg littermates. This independent Tg19959 line derives from the same transgene construct as TgCRND8 (APP695, K670N/M671L+V717F) and has similar levels of APP holoprotein expression and associated pathology but is maintained on a different genetic background (129SvEv/Tac). All animals were bred at the Center for Research in Neurodegenerative Diseases.

Tissue Preparation—Animals were killed by cervical dislocation; brains were removed and bisected at the midline. The left half of the brain was covered in OCT medium and frozen on dry ice; the right half was placed in cold 3% paraformaldehyde in 0.1 M phosphate-buffered saline for fixation, then dehydrated and embedded in paraffin. For general examination of tissue pathology prior to data collection, paraffin-embedded sections were stained with hematoxylin and eosin, modified Bielschowsky silver stain, and Congo red. Immunohistochemical staining with antibodies to tau and ubiquitin was also performed. The animals were treated in accordance with the guidelines of the Canadian Council on Animal Care, and the protocols were approved by the University of Toronto and University of Manitoba.

For infrared and Raman microspectroscopy, the unfixed, flash-frozen tissues were cryosectioned at 8 μm thickness and mounted on either IR reflective slides (Low-e MirriRTM, Kevley Technologies, Chesterland, OH) or gold-coated silicon chips, fabricated in-house at the Synchrotron Radiation Center.

Post-mortem Human Autopsy Tissue—In a pilot study, anonymized samples of hippocampus were acquired prospectively from hospital autopsies at the Health Sciences Center (Winnipeg, Canada) within the scope of the autopsy permission forms and the Autopsy Act. The study was approved by the tissue access committee. Initial assessments (two AD and two non-demented) were made from the available information: age, history of dementia or other neurological disease including seizures, and interval between death and

* This work was supported by the Canadian Institutes of Health Research, the Manitoba Health Research Council (MHRC), and the Natural Sciences and Engineering Research Council (NSERC) Canada. The costs of publication of this article were defrayed in part by the payment of page charges. This article must therefore be hereby marked "advertisement" in accordance with 18 U.S.C. Section 1734 solely to indicate this fact.

[†] Co-first authors.

² Supported through an MHRC fellowship.

³ Supported through an NSERC PGS-A scholarship, a University of Manitoba graduate fellowship, and the McCrorie-West Family Fellowship for Alzheimer Research.

⁴ Dr. Del Bigio holds the Canada Research Chair in Developmental Neuropathology.

⁵ To whom correspondence should be addressed: Dept. of Chemistry, University of Manitoba, 350 Parker Bldg., Winnipeg, Manitoba R3T 2N2, Canada. Tel.: 204-474-6262; Fax: 204-474-7608; E-mail: kmgough@ms.umanitoba.ca.

⁶ The abbreviations used are: AD, Alzheimer disease; $A\beta$, β -amyloid; APP695, amyloid precursor protein; NFT, neurofibrillary tangle; FTIR, Fourier transform infrared; Cr, creatine; PCr, phosphocreatine; CK, creatine kinase; MRS, magnetic resonance spectroscopy; Tg, transgenic.

autopsy. After dissection of the temporal lobe to expose the hippocampus, multiple coronal slices (3–4-mm-thick) were obtained by sharp dissection, frozen immediately by immersion of the sealed container in isopentane cooled in liquid nitrogen, and stored at -70°C .

The remaining brain was fixed by immersion in 10% buffered formalin for 10–14 days, then samples of the contralateral and remaining ipsilateral hippocampus, lateral frontal cortex, and middle temporal gyrus, as well as other brain regions, were obtained and embedded in paraffin. The sections were stained with the modified Bielschowsky method, and Congo red, to diagnose Alzheimer disease according to the NIA-Reagan criteria (16). Both the plaque scores and the NFT percentages were considered in this classification. Following identification of acceptable normal and disease cases, frozen hippocampus sections were warmed to about -30°C , sectioned for microspectroscopy as above, and air-dried.

IR Microspectroscopy—All spectra were collected in reflectance mode from $4000\text{--}700\text{ cm}^{-1}$ at 4 cm^{-1} resolution with Happ-Genzel apodization and saved in $\log(1/R)$ format; thus these are raw data without any other post-processing. Synchrotron data were recorded on a Nicolet Magna 500 FTIR with Nic-Plan IR microscope (Synchrotron Radiation Center, University of Wisconsin) or a Nicolet Magna 860 FTIR with Spectra Tech Continuum IR microscope (National Synchrotron Light Source, Brookhaven National Laboratories). Maps were analyzed with OMNIC/AtIus software (ThermoNicolet). Additional survey maps were acquired on a Bruker Tensor 27 FTIR with Bruker Hyperion microscope (in-house) and analyzed with CytoSpec software (17). Pixel size in IR maps was $6 \times 6\ \mu\text{m}^2$ (National Synchrotron Light Source), $10 \times 10\ \mu\text{m}^2$ (Synchrotron Radiation Center), or $20 \times 20\ \mu\text{m}^2$ (in-house).

IR Spectral Analysis—IR spectroscopy can be used to study protein aggregation, since the position of the amide I band is dependent on the secondary structure of the protein (7, 18–20). Plaques were identified by the presence of a low frequency absorption (1635 cm^{-1}) in the amide I band (7). Reference spectra of pure Cr (Sigma) were recorded in reflectance mode on MirrIR slides.

Raman Microspectroscopy—Spectra of the crystalline inclusions in TgCRND8 mouse brain and human AD brain sections, and of pure Cr (Sigma) mounted on gold-coated silicon chips, were recorded with a Renishaw Raman microscope (Saskatchewan Structural Sciences Centre, University of Saskatchewan); illuminated with 5 milliwatts of 785-nm light, at one-micron spatial resolution and 4 cm^{-1} spectral resolution.

RESULTS

Paraffin-embedded sections from the brains of the TgCRND8 mice and non-transgenic littermate controls were first evaluated by histochemistry and immunohistochemistry (data not shown). No neurofibrillary tangles were apparent in either silver-stained or tau-immunostained sections. Subjectively, in the 21- and 47-week-old transgenic mice, plaques were most abundant in the cerebral cortex, corpus callosum, and hippocampus, slightly less abundant in the striatum and thalamus, and rare in the olfactory bulb, brainstem, and cerebellum. We found plaques in all seven TgCRND8 mice and none in the controls.

We discovered spectral anomalies atypical of both normal and plaque tissue in several IR maps of TgCRND8 brain (Fig. 1A). The sharp spectral bands (Fig. 1A, red) indicated a high degree of order in the material, suggesting a crystalline nature. An IR spectral data base search targeted Cr as a candidate; we confirmed this identity by IR spectroscopy of pure Cr (Fig. 1A, green). The spectrum of the crystalline inclusion embedded in the tissue is readily seen to exhibit all the characteristic peaks of pure Cr, superimposed on the spectrum of normal tissue (Fig. 1A, blue). The identity was confirmed by Raman microspectroscopy of crystalline inclusions in human AD and TgCRND8 hippocampus, which are compared with the Raman spectrum of pure Cr in Fig. 1B. Given the specificity of the number, position, and relative intensity of the spectral bands in these samples, no other assignment is possible. Moreover, there is no evidence of the PCr form, as typical phosphate bands are absent. For Cr detection in the IR maps, we used the integrated intensity of the sharp band appearing at 1304 cm^{-1} , since it lies in a region that is relatively free of interfering bands in normal tissue and can be readily identified. For each pixel that tested positive, the entire spectrum was reviewed to confirm that it was a complete match.

Subsequent re-examination of all maps revealed some intriguing results. Numerous deposits were identified in the cortex of one of the 21-week-old TgCRND8 mice (Fig. 2, A–C). Cr deposits were discovered in the caudate, cortex, and hippocampus of all four of the 47-week-old TgCRND8 mice. About one-third of these were intimately associated with plaques (Fig. 2, D–I);

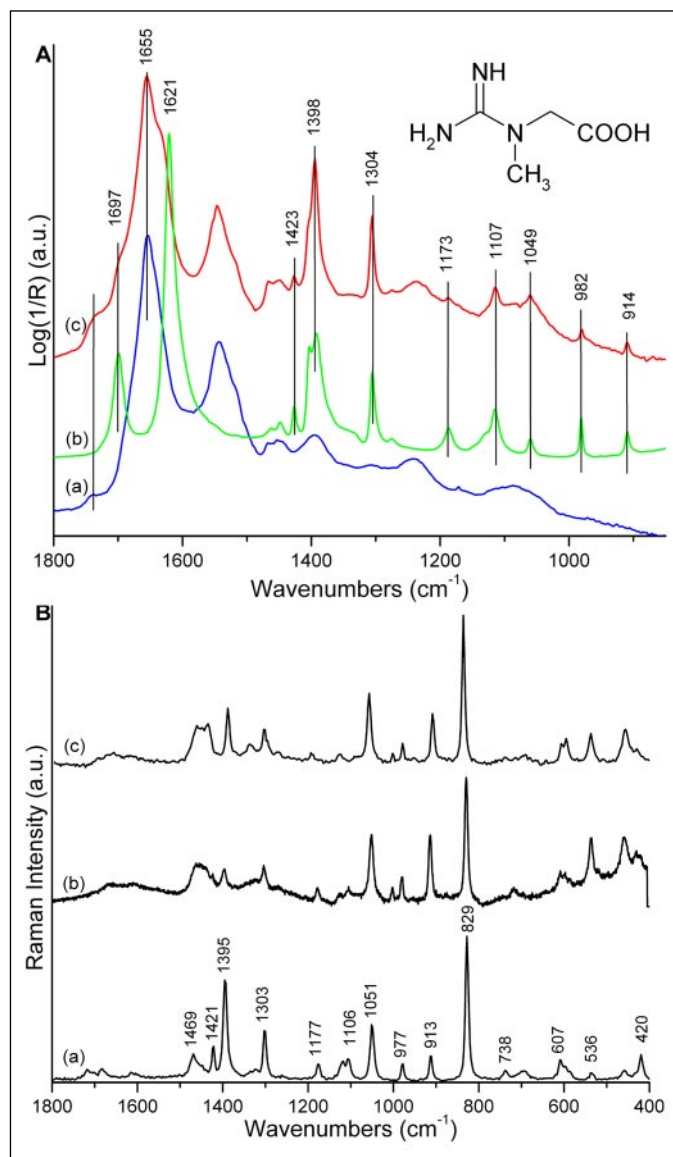


FIGURE 1. Spectra of normal tissue and pure creatine confirm presence of creatine in AD brain tissue. A, FTIR spectrum in the $1900\text{--}800\text{ cm}^{-1}$ fingerprint region of a crystalline inclusion embedded in brain tissue (red) corresponds to the sum of spectra from pure creatine (green) and neuropil (blue). Vertical lines show the correspondence between the signature lines of pure creatine and the matching lines in the AD tissue spectrum. The integrated intensity of the 1304 cm^{-1} band was used to locate creatine in all IR maps. Any spectrum that showed positive was examined to confirm that the entire signature was present. B, the Raman scattering spectrum from $1800\text{--}400\text{ cm}^{-1}$ of crystalline inclusions in hippocampal tissue sections from AD human (top) and Tg mouse brain (middle) compared with that of pure creatine (bottom). All the creatine bands are present in the human and mouse crystalline deposits; a few additional weak bands not seen in the pure creatine spectrum also appear in ordinary tissue and may be disregarded.

the remainder occurred as isolated microdeposits ($10\text{--}20\ \mu\text{m}$ diameter). One crystal was found beside one of the rare dense-cored plaques in the caudate of a 47-week-old TgCRND8. No such deposits were identified in any of the maps from the nine control samples (21 and 47 weeks) or in the other two 21-week-old TgCRND8 animals.

To better evaluate this anomalous Cr presence and its association with the transgenic mice, we conducted a second series of studies. These were expanded to include analysis of the entire hippocampal region in six pairs of TgCRND8 and non-Tg littermates and two pairs from a second Tg line, Tg19959 (8).

The IR signature of Cr was detected in the hippocampus of every Tg mouse, from both lines. No Cr was detected in the young non-transgenic TgCRND8 littermates; a small deposit was identified in three of four controls sacrificed

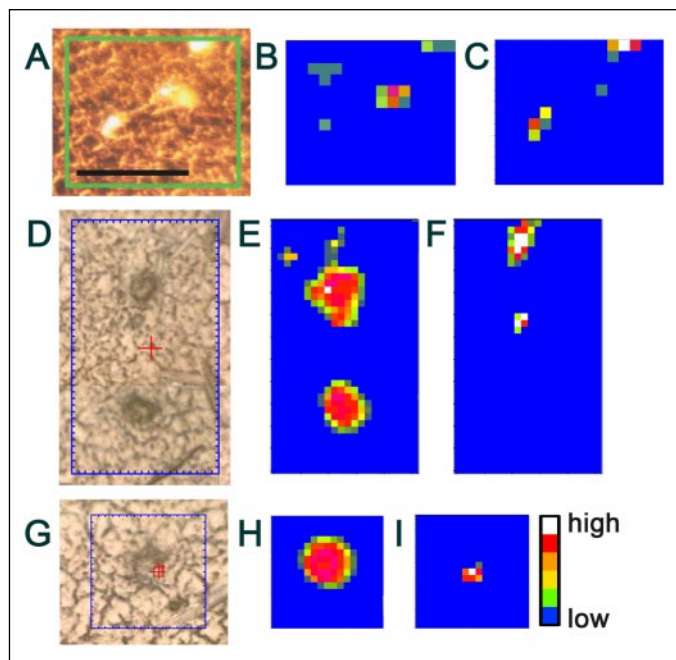


FIGURE 2. Crystallized deposits of creatine are found in cortex of TgCRND8 mouse brain. A, CCD image of cortex tissue from 21-week-old brain mounted on gold-coated silicon wafer (A), and 47-week-old brain on MirrIR slides (D, G) showing the location of the IR map (blue outline). Dense-cored plaques are visible in each map region. Intensities of spectral marker bands are shown with a color scale from high (red) to absent (blue-green) to show either (B, E, H) β -sheet (plaque) or (C, F, I) crystalline deposits of creatine adjacent to plaques. Data were collected at the National Synchrotron Light Source; A–C, IR pixel edge = $10 \times 10 \mu\text{m}$; D–I, pixel edge = $6 \mu\text{m}$. Scale bar = $100 \mu\text{m}$.

after 15 months. Cr was detected throughout the 34-week-old Tg19959 brain (Fig. 3, A and B), while none could be detected in the non-Tg littermate brain (Fig. 3, C and D). A few pixels (6 of 3724) were positive for Cr in the 38-week-old non-Tg brain. In 72-week-old TgCRND8 mice, one Cr deposit was found spreading across an area of $400 \times 60 \mu\text{m}$ in the stratum radiatum, along with numerous smaller deposits scattered throughout the hippocampus (Fig. 3, E and F). A small deposit of Cr was detected around the CA2 of the 72-week-old (Fig. 3G,H) and 89-week-old non-Tg animals.

Finally, we surveyed hippocampal sections from human brain (two AD and two non-demented). The human hippocampus is far larger than the mouse; thus only portions of the brain were surveyed, representative of CA1–4, molecular layer, and dentate gyrus. The IR signature of Cr was detected in sections from all brains, but the occurrence and intensity of the signal were greater in the hippocampus of an advanced AD brain. Representative maps of the CA1 show strong Cr signals detected in 8% of pixels in a CA1 map (Fig. 4, A and B) and only traces in the non-demented (Fig. 4, C and D). Since the intensity of the IR signal is directly proportional to the amount present, we can state with confidence that the amount of Cr present in these AD hippocampus sections was elevated in a manner that was very similar to that found in the Tg mouse model.

DISCUSSION

Creatine is a normal component of brain tissue with an estimated average concentration of $12 \mu\text{M/g}$ wet weight in mouse brain (21). The Cr-PCr system plays a crucial role in energy metabolism, maintaining ATP homeostasis through the enzymatic additional or removal of phosphate (9). The fact that the spectra correspond to Cr and not PCr is reasonable, since all PCr would be depleted at death, leaving Cr as the only existing form. While there is no obvious reason for Cr to be deposited in the AD brains, it is important to note that reduced brain metabolism is almost always associated with AD and other forms of dementia (3). CK has been identified as a target of post-translational oxidative modification in AD brain tissue (10). As an antioxidant with a crucial role in energy metabolism, Cr has been suggested as a potential therapy for AD (9, 22, 23). Furthermore, the analysis of neural cell cultures has shown that Cr concentration in oligodendrocytes and cortical astrocytes is greater than in neurons (24, 25). The TgCRND8 mouse brain showed an inflammatory

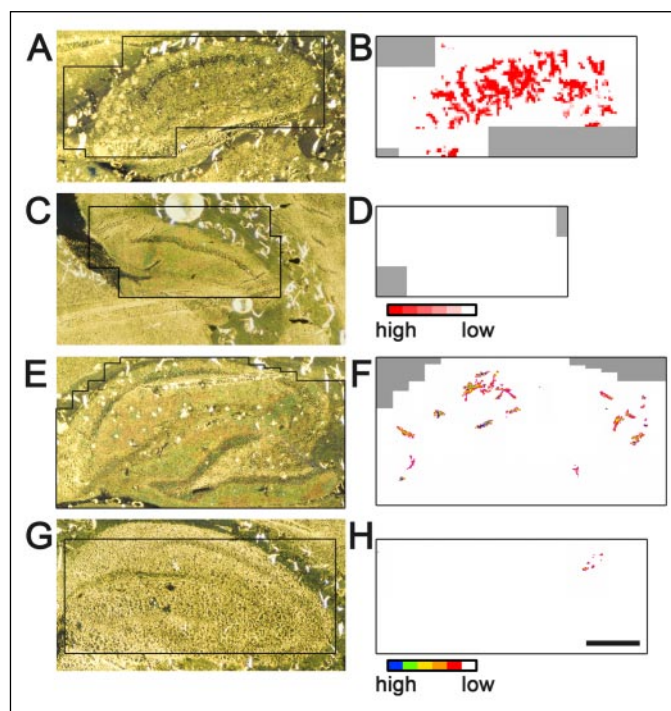


FIGURE 3. Creatine is found in hippocampus of both lines of Tg(K670N/M671L and V717F) mice but not in non-transgenic litter mates. Photomicrographs show mouse brain mounted on gold-coated silicon wafer ($4\times$ magnification); the mapped area is outlined in black, and processed IR maps are shown. Dense-cored plaques scatter white light and are easily visible in reflectance-mode photomicrographs. A, photomicrograph of 34-week-old Tg19959; B, corresponding IR maps processed for creatine. C and D, non-Tg littermate, photomicrograph and IR maps, respectively. Maps were recorded on benchtop Bruker Hyperion; pixel edge = $20 \mu\text{m}$; the monochrome color scale is from high (deep red) to absent (white). E, photomicrograph of 72-week-old TgCRND8; G, corresponding IR maps processed for creatine. C and D, non-Tg littermate, photomicrograph and IR maps, respectively. The color scale is from high (blue) to low (red) or absent (white). Maps recorded at the Synchrotron Radiation Center with NicPlan microscope; pixel edge = $10 \mu\text{m}$. Scale bar = $500 \mu\text{m}$.

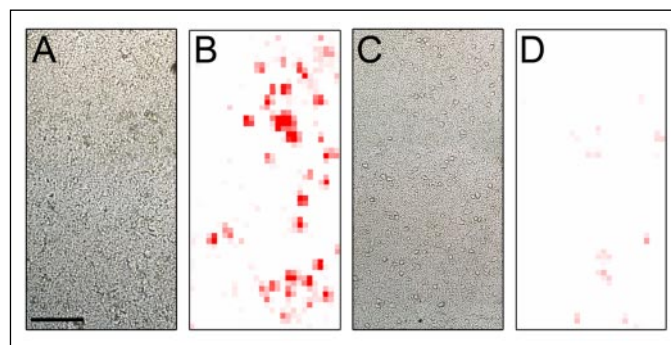


FIGURE 4. Creatine is detected in AD but not in non-demented post-mortem human hippocampus. Photomicrographs of post-mortem human hippocampus, CA1 region, mounted on MirrIR slides ($10\times$ magnification). A and B, AD brain tissue and corresponding IR map processed for creatine. C and D, photomicrograph of non-demented brain and corresponding processed IR map. Maps were recorded on benchtop Bruker Hyperion; pixel edge = $20 \mu\text{m}$; the color scale is the same as described for Fig. 3, B and D. Scale bar = $200 \mu\text{m}$.

response accompanied by microglial activation (8) that may be associated with the Cr deposits found here.

The FTIR detection method employed here is critical to our discovery. These small, soluble deposits would be removed by the repetitive solvent treatments and washes employed in standard staining procedures. Under our protocols, the frozen, unfixed tissue is cryosectioned, and the mounted sections are desiccated in air. Thus, the content of the sample is unaltered in that nothing has been added or taken away (except water). We note that there is no likelihood of contamination: tissues from control and AD brain were processed at the same time. The same result was obtained when sections from Tg

and non-Tg mouse brain were mounted on different substrates (MIRR and gold-coated silicon). We have used animals from two different lines such that the doubly mutant APP695 is maintained on different genetic backgrounds. The only occurrences of Cr in a non-Tg mouse brain were relatively minor deposits, found in the extremely aged animals (89 and 72 weeks, Fig. 3G,H), and traces in the 38-week-old non-Tg19959 littermate brain. This indicates a gradual, age-dependent increase in oxidative stress. The distribution in the human tissue is similar to that in the Tg mouse; it is sometimes associated with a plaque but frequently is widespread randomly across the tissue areas.

In magnetic resonance spectroscopy (MRS), the Cr/PCr signal has been used extensively as an internal standard relative to which the concentrations of other components (e.g. *N*-acetylaspartate, choline, myo-inositol, and glutamate-glutamine complex) have been estimated (26). However, a quantitative analysis reported elevated levels of Cr in the gray and white matter of elderly and AD patients compared with young controls (27). *In vivo* (28) and *ex vivo* (29) MRS studies pointed out the strong heterogeneity of the elderly subjects and could not conclusively differentiate between AD and aged matched controls based on the Cr content. However, a 1–2 mM elevation of Cr was found in the five most severe AD cases in an *in vivo* study (30) of 21 AD patients and 17 age-matched controls. Voxels were $2.0 \times 2.0 \times 2.0 \text{ cm}^3$. We have found varying amounts of Cr in the human autopsy samples, but the small sample size precludes any detailed conclusions on its relationship to the disease evolution. Cr is likely an indicator of oxidative stress and thus may be associated with many different conditions in humans. The extensive microdeposits of Cr found in the Tg mice and the small localized deposits found in the hippocampus of our most aged control mice mirror the results from the MRS studies.

The spatial resolution of MRS experiments is insufficient to detect the localized nature of the deposits found here; relative concentration estimates are frequently based on the assumption that the average Cr concentration is constant. The striking and unexpected discovery reported here casts doubt on this assumption and bears further detailed investigation. Many other intriguing questions are raised by this discovery, including the form and micro-localization of the Cr *in vivo* and the possible disease-associated pathways that control this accumulation.

Acknowledgments—We thank Dr. M. Mayne for assistance in animal management and R. Strome for Tg19959 mice. We thank Drs. L. Miller, L. Carr, and N. Marinkovic (National Synchrotron Light Source) and P. Dumas (Soleil, France); Dr. R. Sammynaiken (Saskatchewan Structural Sciences Centre, University of Saskatchewan); S. Allen, A. Bookatz, Dr. F. Hawthorne, A. Holliday, S. Janeczko, Dr. S. Mai, M. Ogg, C. Taylor-Kashton, and F. Zeiler (University of Manitoba) for technical assistance.

REFERENCES

- Selkoe, D. J. (2001) *Physiol. Rev.* **81**, 741–766
- Beal, M. F. (1995) *Ann. Neurol.* **38**, 357–366

- Blass, J., Gibson, G. E., and Hoyer, S. (2002) *J. Alzheimer Dis.* **4**, 225–232
- Munch, G., Schinzel, R., Loske, C., Wong, A., Durany, N., Li, J. J., Vlassara, H., Smith, M. A., Perry, G., and Riederer, P. (1998) *J. Neural Transm.* **105**, 439–461
- Gibson, G. E. (2002) *Free Radic. Biol. Med.* **32**, 1061–1070
- Butterfield, D. A., and Castegna, A. (2003) *Appl. Genomics Proteomics* **2**, 67–70
- Gough, K. M., Rak, M., Bookatz, A., Del Bigio, M., Mai, S., and Westaway, D. (2005) *Vib. Spectrosc.* **38**, 133–141
- Chishti, M. A., Yang, D., Janus, C., Phinney, A. L., Horne, P., Pearson, J., Strome, R., Zuker, N., Loukides, J., French, J., Turner, S., Lozza, G., Grilli, M., Kunicki, S., Morissette, C., Paquette, J., Gervais, F., Bergeron, C., Fraser, P. E., Carlson, G. A., St. George-Hyslop, P., and Westaway, D. (2001) *J. Biol. Chem.* **276**, 21562–21570
- Wyss, M., and Kaddurah-Daouk, R. (2000) *Physiol. Rev.* **80**, 1107–1213
- Castegna, A., Aksenov, M., Aksenova, M., Thongboonkerd, V., Klein, J. B., Pierce, W. M., Booze, R., Markesbery, W. R., and Butterfield, D. A. (2002) *Free Radic. Biol. Med.* **33**, 562–571
- David, S., Shoemaker, M., and Haley, B. E. (1998) *Mol. Brain Res.* **54**, 276–287
- Aksenov, M., Aksenova, M., Butterfield, A., and Markesbery, W. R. (2000) *J. Neurochem.* **74**, 2520–2527
- Aksenov, M. Y., Aksenova, M. V., Markesbery, W. R., and Butterfield, D. A. (1998) *J. Mol. Neurosci.* **10**, 181–192
- Mark, R. J., Pang, Z., Geddes, J. W., Uchida, K., and Mattson, M. P. (1997) *J. Neurosci.* **17**, 1046–1054
- Casley, C. S., Canevari, L., Land, J. M., Clark, J. B., and Sharpe, M. A. (2002) *J. Neurochem.* **80**, 91–100
- The National Institute on Aging and Reagan Institute Working Group on Diagnostic Criteria for the Neuropathological Assessment of Alzheimer's Disease (1997) *Neurobiol. Aging* **18**, S1–S2
- Lasch, P., Haensch, W., Naumann, D., and Diem, M. (2004) *Biochim. Biophys. Acta* **1688**, 176–186
- Gough, K. M., Zelinski, D., Wiens, R., Rak, M., and Dixon, I. M. C. (2003) *Anal. Biochem.* **316**, 232–242
- Choo, L. P., Wetzel, D. L., Halliday, W. C., Jackson, M., LeVine, S. M., and Mantsch, H. H. (1996) *Biophys. J.* **71**, 1672–1679
- Seshardi, S., Khurana, R., and Fink, A. L. (1999) *Methods Enzymol.* **309**, 559–579
- Ipsiroglu, O. S., Stromberger, C., Ilas, J., Hoger, H., Muhl, A., and Stockler-Ipsiroglu, S. (2001) *Life Sci.* **69**, 1805–1815
- Tarnopolsky, M. A., and Beal, F. M. (2001) *Ann. Neurol.* **49**, 561–574
- Wyss, M., and Schulze, A. (2002) *Neuroscience* **112**, 243–260
- Urenjak, J., Williams, S. R., Gadian, D. G., and Noble, M. (1993) *J. Neurosci.* **13**, 981–989
- Dringen, R., Verleysdonk, S., Hamprecht, B., Willker, W., Leibfritz, D., and Brand, A. (1998) *J. Neurochem.* **70**, 835–840
- Valenzuela, M. J., and Sachdev, P. (2001) *Neurology* **56**, 592–598
- Pfefferbaum, A., Adalsteinson, E., Spielman, D., Sullivan, E. V., and Lim, K. O. (1999) *Arch. Gen. Psychiatry* **56**, 185–192
- Stoppe, G., Bruhn, H., Pouwels, P. W. J., Hanicke, W., and Frahm, J. (2000) *Alzheimer Dis. Assoc. Disord.* **14**, 112–119
- Mohanakrishnan, P., Fowler, A. H., Vonsattel, J. P., Jolles, P. R., Husain, M. M., Liem, P., Myers, L., and Komoroski, R. A. (1998) *J. Gerontol. A Biol. Sci. Med. Sci.* **52**, B111–B117
- Huang, W., Alexander, G. E., Chang, L., Shetty, H. U., Krasuski, J. S., Rapoport, S. I., and Schapiro, M. B. (2001) *Neurology* **57** 626–632